Method to Determine the Recombination Characteristics of Minority Carriers in Graded-Band-Gap Solar Cells

Choong-Heui Chung*

Department of Materials Science and Engineering, Hanbat National University, Daejeon 34158, Republic of Korea

(Received 8 March 2019; revised manuscript received 30 July 2019; published 28 August 2019)

Graded-band-gap solar cells have been shown to be a promising way of improving the power conversion efficiency of solar cells. However, due to the mixture of drift and diffusional motion of charge carriers induced by the band-gap grading in the solar cells, existing assessment techniques fail to properly characterize the electrical quality of the graded-band-gap solar cells. I develop a simple method to simultaneously characterize recombination characteristics including the minority carrier diffusion length L_d and the back-surface recombination velocity S_b through depth-resolved minority carrier collection length by diffusion in the graded-band-gap solar cells. The suggested method relies on wavelength-dependent lateral photocurrent in a simple custom-designed device structure, which enables to determine the recombination characteristics of the minority carrier, regardless of the band-gap grading. As a proof of concept, the suggested method is applied to a graded-band-gap $Cu(In, Ga)Se_2$ solar cell without even knowing the depth profile of the band-gap grading. The determined L_d and S_b values match well with previous reports of these values for $Cu(In, Ga)Se_2$ solar cells. This result suggests that this approach can be thus readily extended to other types of solar cells because this approach does not require the depth profile of the band-gap grading.

DOI: 10.1103/PhysRevApplied.12.024060

I. INTRODUCTION

Graded-band-gap light absorbers have been utilized to improve the power conversion efficiency of thin-film solar cells since the 90s. These include $Cu(In, Ga)Se_2$ (CIGS) [1–3], $Cu_2ZnSn(S, Se)_4$ [4,5] and *a*-SiGe:H [6] solar cells. Perovskite solar cells have also recently been employed as a graded-band-gap structure [7–10]. The quasielectric field induced by the proper band-gap grading of the light absorbers induces the drift motion of charge carriers, and thus improves the efficiency of carrier collection. The electronic energy level in a light absorber layer is generally graded by intentional grading of the composition, and also can be altered by fluctuating potentials caused by high-defect density without intentional compositional grading [11–13]. In order to further improve the solar cells' performance, it is critical to identify the electrical quality of the devices. Previous studies have shown that recombination loss mainly occurs mainly either in the light absorber or at the back surface of solar cells [14–16]. The electrical quality of the light absorber can be characterized by the minority carrier diffusion length L_d, and that of the back surface is represented by the back-surface recombination velocity S_b.

Although previous studies have determined L_d [17–23], S_b [24,25], or both [15,16], the results are applicable only to ungraded (i.e., constant in the depth direction) band-gap solar cells, but not to graded-band-gap solar cells. Previously, energy dependent electron-beam-induced current has been used to determine L_d in graded-band-gap CIGS solar cells. However, this technique requires the S_b value as well as the depth profile of the band gap of the light absorber [26]. In ungraded-band-gap solar cells, the charge carriers travel only by diffusion in the neutral region of the light absorber. In contrast, in graded-band-gap solar cells, the charge carriers travel by a mixture of diffusion and drift, which makes it difficult to determine the characteristic properties of diffusion alone (Fig. 1).

This paper presents a simple method for simultaneously determining both L_d and S_b through depth-resolved L_c distribution in solar cells regardless of the band-gap grading where L_c is the minority carrier collection length by diffusion. The determination of L_d and S_b values consists of two steps. First, the depth-resolved L_c profiles are determined by combining the theoretical and the measured depth-dependent lateral photocurrents i_{LP}. Second, both L_d and S_b are determined from the obtained depth-resolved L_c profiles using a relation between L_d, S_b, and L_c. Highly efficient CIGS solar cells have generally been obtained using a grading composition, resulting in a graded-band-gap CIGS layer to improve charge collection efficiency [27,28]. As a proof of concept, this method is successfully applied to a graded-band-gap CIGS solar cell without even knowing the depth profile of the CIGS band gap. The determined

*choong@hanbat.ac.kr

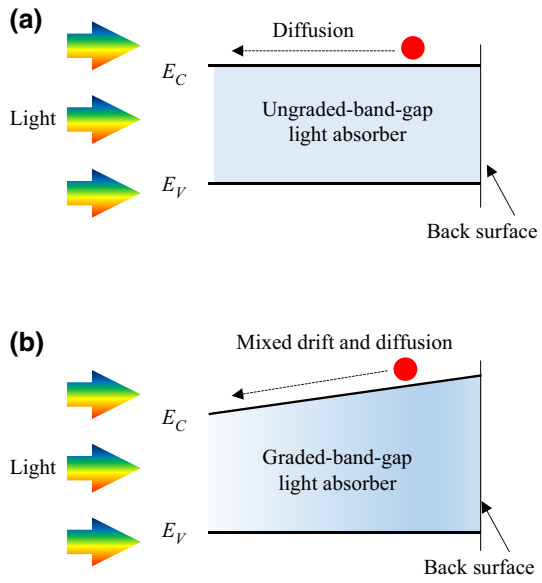

FIG. 1. Illustration of the motion of photogenerated minority carriers in solar cells. (a) Photogenerated minority carriers travel only by diffusion in the neutral region of an ungraded-band-gap light absorber. (b) The minority carriers travel by a mixture of drift and diffusion in the neutral region of a graded-band-gap light absorber.

L_d and S_b values match previous reports of these values for CIGS solar cells [19,26,29,30]. This approach can be readily extended to other types of solar cells because it does not require the depth profile of the band gap of a light absorber.

It is useful to make a clear difference between three kinds of diffusional lengths for the minority carriers used in this work: (1) the minority carrier diffusion length L_d, (2) the effective minority carrier diffusion length L_{eff}, and (3) the minority carrier collection length by diffusion L_c. First, L_d is defined by the average magnitude of diffusional displacement that the minority carriers move before they recombine only in the bulk of a light absorber. Thus it is given by $L_d = \sqrt{D\tau_b}$, where D is the diffusivity of the minority carrier and τ_b is the bulk life time of the carrier. However, the recombination of the minority carriers occurs simultaneously mainly both in the bulk of light absorber and at the back surface. Second, L_{eff} is thus defined by the average magnitude of diffusional displacement of the minority carriers between generation and recombination that occurs at both the bulk and at the back surface [31]. It is thus given by $L_{\text{eff}} = \sqrt{D\tau_{\text{eff}}}$. The effective life time is τ_{eff} with a relation of $(1/\tau_{\text{eff}}) = (1/\tau_b) + (1/\tau_s)$, where τ_s is the back-surface life time. L_{eff} is affected by both L_d and S_b [3,4]. Finally, L_c is introduced to make the collection probability of photogenerated minority carriers be $\eta = \exp(-|\overrightarrow{\Delta_{\text{diff}}}|/L_c)$, where $|\overrightarrow{\Delta_{\text{diff}}}|$ is the magnitude of the diffusional displacement of the carrier to be collected as photocurrent. Let us now take a look at the relationships between L_d, L_{eff}, and L_c. When the back surface negligibly affects the recombination, $L_d \cong L_{\text{eff}}$. In a one-dimensional diffusion situation, $L_{\text{eff}} \cong L_c$. $L_d \cong L_{\text{eff}} \cong L_c$ when the back surface negligibly affects the recombination and the carriers also diffuse in one dimension [15,19,21,32].

II. STRATEGY FOR DETERMINING L_C DEPTH PROFILES IN GRADED-BAND-GAP SOLAR CELLS

As a procedure to determine depth-resolved L_c profiles, we first consider the analysis of the generic test structure illustrated in Fig. 2. The depth-sensitive collector of photogenerated minority carriers consists of a three-layer structure composed of a bottom electrode, a vertically graded-band-gap light absorber, and a top electrode. The light absorber is partially covered by an opaque and top electrode, which functions as a collector of photogenerated minority carriers. Because this top electrode is opaque to incident light, it masks the entire region beneath it, and therefore, charge carriers are generated only outside its periphery. To obtain the diffusional characteristic L_c values, it is required to separate out diffusion and drift motion in a graded-band-gap light absorber. For the photogenerated minority carrier to be collected, it is necessary to have a total displacement $\overrightarrow{\Delta_{\text{total}}}$, whose magnitude is the shortest distance from the generation position to the charge collector (Fig. 2). The photogenerated carriers travel by both diffusion and drift, satisfying $\overrightarrow{\Delta_{\text{total}}} = \overrightarrow{\Delta_{\text{drift}}} + \overrightarrow{\Delta_{\text{diff}}}$, where $\overrightarrow{\Delta_{\text{drift}}}$ is the displacement of the carriers by drift and $\overrightarrow{\Delta_{\text{diff}}}$ is the diffusional displacement.

The L_c value is determined by combining the theoretical and the measured i_{LP} values. A theoretical prediction of photocurrent $i_{\text{LP}} = i_{\text{LP}}(L_c)$ is made and the i_{LP} value is then measured for this test structure under monochromatic light illumination. The depth dependency of L_c comes from varying the wavelength of the incident light (and thus the device penetration depth). Theoretically predicting $i_{\text{LP}} = i_{\text{LP}}(L_c)$ requires the $|\overrightarrow{\Delta_{\text{diff}}}|$ value to calculate $\eta = \exp(-|\overrightarrow{\Delta_{\text{diff}}}|/L_c)$ with a condition of $\overrightarrow{\Delta_{\text{total}}} = \overrightarrow{\Delta_{\text{drift}}} + \overrightarrow{\Delta_{\text{diff}}}$. To this end, the band-gap depth profile of the light absorber and the drift mobility of the minority carrier are required. However, the derived equation $i_{\text{LP}} = i_{\text{LP}}(L_c)$ is only specific to each type of graded-band-gap solar cell because each type of cell will have different values for both the band-gap depth profile and the drift mobility. Ideally, the derived relationship should be generic and applicable to different solar cells.

However, we maintain generality by theoretically deriving the functions $i_{\text{LP}} = i_{\text{LP}}(L_c)$ for two extreme cases: case I of $|\overrightarrow{\Delta_{\text{drift}}}| = 0$, that is, the maximum $|\overrightarrow{\Delta_{\text{diff}}}|$, and case II of $|\overrightarrow{\Delta_{\text{drift}}}| = z$, that is, the minimum $|\overrightarrow{\Delta_{\text{diff}}}|$. The real $|\overrightarrow{\Delta_{\text{drift}}}|$ for a particular solar cell will be positioned somewhere between $|\overrightarrow{\Delta_{\text{drift}}}| = 0$ and $|\overrightarrow{\Delta_{\text{drift}}}| = z$ (Fig. 2). Based on the

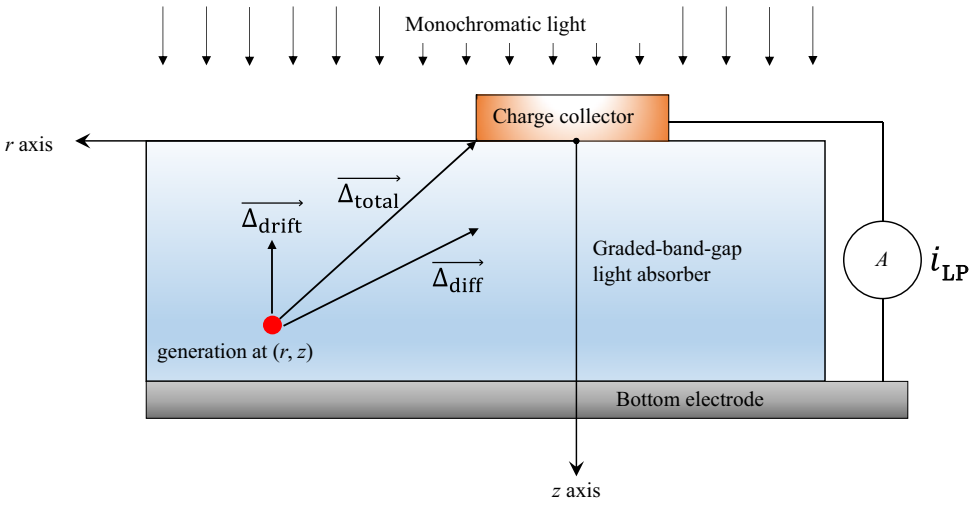

FIG. 2. Illustration of the motion of photogenerated minority carriers in a graded-band-gap light absorber. The charge carriers travel by a mixture of diffusion and drift to reach the nearest point of a charge collector. $\overrightarrow{\Delta_{total}}$ is the total displacement, whose magnitude is the shortest distance from the generation position to the charge collector. $\overrightarrow{\Delta_{drift}}$ is the displacement by drift and $\overrightarrow{\Delta_{diff}}$ is the diffusional displacement. $\overrightarrow{\Delta_{total}} = \overrightarrow{\Delta_{drift}} + \overrightarrow{\Delta_{diff}}$. Thus, it will be $0 \leq |\overrightarrow{\Delta_{drift}}| \leq z$.

functions $i_{LP} = i_{LP}(L_c)$ derived for the two cases and the i_{LP} values measured for the particular solar cell by varying the wavelength of the incident light, two L_c depth profiles are extracted. Although not all of the two L_c depth profiles provide the real L_c depth profile for a particular solar cell, they are able to provide the range in which the real L_c depth profile lies. When tested, this approach provides reasonable L_d and S_b values for the fabricated graded-band-gap CIGS solar cell without even knowing the depth profile of the CIGS band gap, as discussed in Sec. IV. This result shows that the suggested approach is generic and applicable to different solar cells, one of the most significant aspects of this work.

It is worth noting that the deduced L_c is not truly depth resolved because the depth position of photogenerated minority carriers continuously changes from z to 0 between generation and collection (Fig. 2). Thus, the determined L_c should not be taken as the value at a specific depth in a light absorber, but rather as the average over the layer below the penetration depth [33]. It has been reported that this approach causes uncertainties in the measured values to be estimated of approximately 10% [34]. Thus, the L_c values inferred in this work can be considered to be a good approximation of the real distribution.

III. DERIVATION OF FUNCTION $i_{LP} = i_{LP}(L_C)$

Let us derive the mathematical expression $i_{LP} = i_{LP}(L_c)$ for the two extreme cases with a custom-designed test structure described in more detail [Fig. 3(a)]. The space charge region (SCR) extends to the side at the edge of the top electrode and is assumed to be a quarter circle with a radius of the SCR width W [35]. Equations (7) and (11) for $i_{LP} = i_{LP}(L_c)$ are derived for case I and case II, respectively. Derivation details can be found in the following.

The intensity $dI_{ab}(z)$ of absorbed light at a depth of $z \sim z + dz$ in regions that are not masked by the top electrode is expressed by the Beer-Lambert law

$$dI_{ab}(z) = I_L(1 - R_{ab})\alpha \exp(-\alpha z)dz, \tag{1}$$

where I_L is the intensity of the incident light, R_{ab} is the reflectance from the front surface of the light absorber layer due to the different refractive indices between air and the absorber layer, and α is the absorption coefficient of the light absorber. The number of photogenerated charge carriers per unit time within an annulus of radius r, width dr, and thickness dz in cylindrical coordinates [Fig. 3(b-i)] can thus be written

$$dN(z) = \frac{dI_{ab}(z)}{(hc/\lambda)} 2\pi r dr, \tag{2}$$

where hc/λ is the photon energy, h is Planck's constant, c is the speed of light, and λ is the wavelength.

A. Function $i_{LP} = i_{LP}(L_c)$ for case I

Case I corresponds to the maximum diffusional displacement for photogenerated minority carriers to be collected. The charge carriers are generally assumed to be completely collected in the SCR [22,23]. Therefore, the maximum diffusional displacement to reach the nearest point on the boundary of the SCR is $|\overrightarrow{\Delta^{I}_{diff}}| = \sqrt{(r - r_o)^2 + z^2} - W$ for the carriers generated at a location (r, z) outside the SCR [Fig. 3(b-ii)]. The collection probability functions $\eta(r, z)$ are thus summarized as follows:

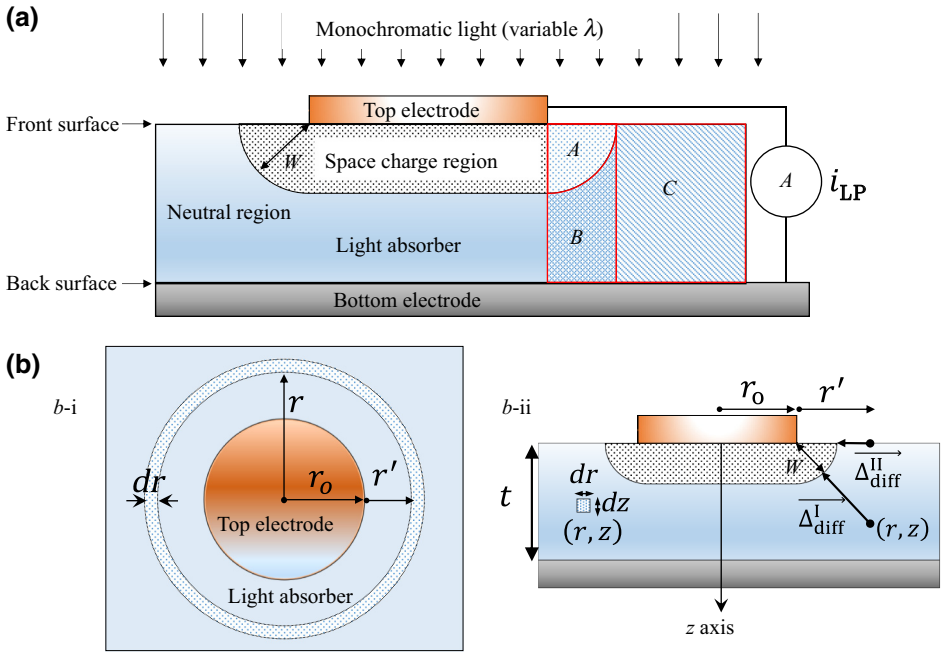

FIG. 3. Illustration of the device design for the theoretical prediction of $i_{LP} = i_{LP}(L_c)$ and the measurement of i_{LP} to determine L_c. (a) Cross-section schematic of a three-layer test structure composed of a bottom electrode, an interlayer light absorber, and a top electrode. The space charge region and zones A, B, and C are marked. (b) An annulus with radius r, width dr, and thickness dz in cylindrical coordinates is shown in (i) top view and (ii) cross-section view of the test pattern. The maximum $\overrightarrow{\Delta^{I}_{diff}}$ and minimum $\overrightarrow{\Delta^{II}_{diff}}$ of diffusional displacement for charge carriers generated at (r, z) outside the photogenerated charge outside the space charge region are marked at (b-ii).

$$\eta(r,z) = \begin{pmatrix} 1 & \text{for zone } A\text{: } (r-r_o) < W \text{ and } z < \sqrt{W^2-(r-r_o)^2} \\ \exp\left(-\frac{\sqrt{(r-r_o)^2+z^2}-W}{L_c}\right) & \text{for zone } B\text{: } (r-r_o) < W \text{ and } z > \sqrt{W^2-(r-r_o)^2} \\ \exp\left(-\frac{\sqrt{(r-r_o)^2+z^2}-W}{L_c}\right) & \text{for zone } C\text{: } (r-r_o) > W \end{pmatrix}. \tag{3}$$

The contribution from an annulus of width dr [Fig. 3(b)] to the total collected current is

$$di(r,z) = edN(z)\eta(r,z). \tag{4}$$

By combining Eqs. (1)–(4), the total lateral photocurrent (i_{LP}) captured into the external circuit is given by

$$\begin{aligned} i_{LP} = i^A_{LP} + i^B_{LP} + i^C_{LP} &= \int_{z=0}^{z=t}\int_{r=r_o}^{r=\infty} di(r,z) \\ &= \frac{2\pi e I_L(1-R_{ab})\alpha\lambda}{hc}\left[\int_{z=0}^{z=\sqrt{W^2-(r-r_o)^2}}\int_{r=r_o}^{r=r_o+W} r\exp(-\alpha z)drdz\right. \\ &+ \int_{z=\sqrt{W^2-(r-r_o)^2}}^{z=t}\int_{r=r_o}^{r=r_o+W} r\exp(-\alpha z)\exp\left(-\frac{\sqrt{(r-r_o)^2+z^2}-W}{L_c}\right)drdz \\ &\left.+ \int_{z=0}^{z=t}\int_{r=r_o+W}^{r=\infty} r\exp(-\alpha z)\exp\left(-\frac{\sqrt{(r-r_o)^2+z^2}-W}{L_c}\right)drdz\right], \end{aligned} \tag{5}$$

where i_{LP}^{A}, i_{LP}^{B}, and i_{LP}^{C} are the photocurrent contributions from zones A, B, and C, respectively. Substituting r' for $r - r_o$ in Eq. (5), we obtain Eq. (6)

$$
\begin{aligned}
i_{\mathrm{LP}} = \frac{2\pi e I_L (1 - R_{\mathrm{ab}})\alpha\lambda}{hc} \Bigg[& \int_{z=0}^{z=\sqrt{W^2 - r'^2}} \int_{r'=0}^{r'=W} (r' + r_o) \exp(-\alpha z) dr' dz \\
& + \int_{z=\sqrt{W^2 - r'^2}}^{z=t} \int_{r'=0}^{r'=W} (r' + r_o) \exp(-\alpha z) \exp\left(- \frac{\sqrt{r'^2 + z^2} - W}{L_c} \right) dr' dz \\
& + \int_{z=0}^{z=t} \int_{r'=W}^{r'=\infty} (r' + r_o) \exp(-\alpha z) \exp\left(- \frac{\sqrt{r'^2 + z^2} - W}{L_c} \right) dr' dz \Bigg]. \qquad (6)
\end{aligned}
$$

More than 99% of i_{LP} comes from the range of $0 \le r' \le W + 5L_c$. W and L_c are on the order of 1 μm in most thin-film solar cells. r_o is arbitrarily experimentally adjustable and is fixed to 1 mm in this work. Therefore, by experimentally setting $r_o \gg W + 5L_c$, we can set $(r' + r_o) \cong r_o$ in the integrals in Eq. (6) to obtain the following equation

$$
\begin{aligned}
& \frac{i_{\mathrm{LP}} hc}{2\pi r_o e I_L (1 - R_{\mathrm{ab}})\alpha\lambda} \\
& = \int_{z=0}^{z=\sqrt{W^2 - r'^2}} \int_{r'=0}^{r'=W} \exp(-\alpha z) dr' dz \\
& \quad + \int_{z=\sqrt{W^2 - r'^2}}^{z=t} \int_{r'=0}^{r'=W} \exp(-\alpha z) \\
& \quad \times \exp\left(- \frac{\sqrt{r'^2 + z^2} - W}{L_c} \right) dr' dz \\
& \quad + \int_{z=0}^{z=t} \int_{r'=W}^{r'=\infty} \exp(-\alpha z) \exp\left(- \frac{\sqrt{r'^2 + z^2} - W}{L_c} \right) dr' dz. \qquad (7)
\end{aligned}
$$

If the $i_{\mathrm{LP}}, r_o, I_L, R_{\mathrm{ab}}, \alpha$, and W values are available, we can determine L_c from Eq. (7). r_o is arbitrarily experimentally adjustable, i_{LP} can be measured using a current meter, I_L can be measured using an optical power meter, R_{ab} can be measured using a UV-Visible spectrometer, and W can be also obtained by the capacitance measurement. The α values, the material properties of light absorbers, are normally available in literature. The term $2\pi r_o$ on the left-hand side of Eq. (7) corresponds to the value for the perimeter of the disk-shaped top electrode. Although a disk-shaped electrode is not essential in principle, this simple geometry is chosen for mathematical convenience in deriving the theoretical prediction. Therefore, for other shapes of the electrode, we can simply replace $2\pi r_o$ with the length of the employed electrode perimeter in the above equation. The arguments presented in this paragraph also apply to Eq. (11) for $i_{\mathrm{LP}} = i_{\mathrm{LP}}(L_c)$ for case II.

B. Function $i_{\mathrm{LP}} = i_{\mathrm{LP}}(L_c)$ for case II

Case II corresponds to the minimum diffusional displacement for photogenerated minority carriers to be collected. All vertical displacement is done by drift for case II. The minimum diffusional displacement for the carriers generated in zones A and B is zero. For photogenerated minority carriers generated in zone C to reach the nearest point on the boundary of the SCR, the minimum diffusional displacement is $|\overrightarrow{\Delta_{\mathrm{diff}}^{\mathrm{II}}}| = r - (r_o + W)$ [Fig. 3(b-ii)]. The $\eta(r, z)$ values are thus summarized as follows:

$$
\eta(r,z) = \begin{pmatrix} 1 & \text{for zone } A \text{ and } B\text{: } (r - r_o) < W \\ \exp\left(- \frac{r - (r_o + W)}{L_c} \right) & \text{for zone } C\text{: } (r - r_o) > W \end{pmatrix}. \qquad (8)
$$

Therefore, the total lateral photocurrent (i_{LP}) captured into the external circuit is given by

$$
\begin{aligned}
i_{\mathrm{LP}} = \int_{z=0}^{z=t} \int_{r=r_o}^{r=\infty} di(r,z) = \frac{2\pi e I_L (1 - R_{\mathrm{ab}})\alpha\lambda}{hc} \\
\times \Bigg[\int_{z=0}^{z=t} \int_{r=r_o}^{r=r_o+W} r \exp(-\alpha z) dr dz \\
+ \int_{z=0}^{z=t} \int_{r=r_o+W}^{r=\infty} r \exp(-\alpha z) \\
\times \exp\left(- \frac{r - (r_o + W)}{L_c} \right) dr dz \Bigg]. \qquad (9)
\end{aligned}
$$

Substituting r' for $r - r_o$ in Eq. (9), we obtain Eq. (10)

$$
\begin{aligned}
i_{\mathrm{LP}} = \frac{2\pi e I_L (1 - R_{\mathrm{ab}})\alpha\lambda}{hc} \\
\times \Bigg[\int_{z=0}^{z=t} \int_{r'=0}^{r'=W} (r' + r_o) \exp(-\alpha z) dr' dz
\end{aligned}
$$

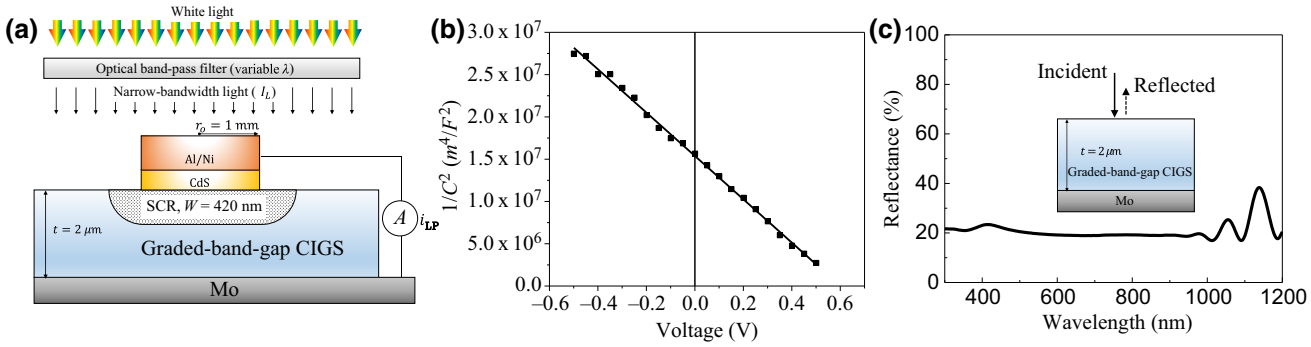

FIG. 4. (a) A cross-section CIGS test pattern for the lateral photocurrent measurement at short circuit under steady-state illumination of narrow-bandwidth light. $t = 2\,\mu$m, $r_o = 1$ mm, and $W = 420$ nm. (b) The Mott-Schottky plot of the CIGS device. (c) The reflectance from the CIGS front surface.

$$+\int_{z=0}^{z=t}\int_{r'=W}^{r'=\infty}(r'+r_o)\exp(-\alpha z)\times\exp\left(-\frac{r'-W}{L_c}\right)dr'dz\Bigg]. \quad (10)$$

Similarly, to obtain Eq. (7) from Eq. (6), we can set $(r' + r_o) \cong r_o$ in the integrals in Eq. (10) to obtain Eq. (11)

$$\frac{i_{\mathrm{LP}}hc}{2\pi r_o eI_L(1-R_{\mathrm{ab}})\alpha\lambda} = \int_{z=0}^{z=t}\int_{r'=0}^{r'=W}\exp(-\alpha z)dr'dz + \int_{z=0}^{z=t}\int_{r'=W}^{r'=\infty}\exp(-\alpha z)\exp\left(-\frac{r'-W}{L_c}\right)dr'dz. \quad (11)$$

The L_c value that most accurately satisfies Eq. (11) is the solution for case II.

IV. APPLICATION TO GRADED-BAND-GAP CIGS SOLAR CELLS

As a proof of concept, the suggested method for measuring the depth-resolved L_c is applied to the case of a graded-band-gap CIGS solar cell.

A. Fabrication and characterization of a CIGS test structure

The CIGS test pattern includes a disk-shaped Al/Ni/CdS collecting electrode on CIGS/Mo [Fig. 4(a)]. CIGS absorber layers with a thickness of $t = 2\,\mu$m are prepared by three-stage coevaporation to produce a graded-band-gap CIGS layer on Mo-coated soda-lime glass. CdS buffer layers are prepared by chemical bath deposition and Al/Ni opaque top electrodes are prepared using e-beam evaporation through a shadow mask. The detailed fabrication procedure can be found elsewhere [36,37]. The CdS buffer layers are removed using wet etching in the test pattern before measuring i_{LP}. The geometrical device parameters are $t = 2\,\mu$m and $r_o = 1$ mm. High-frequency (100 kHz) capacitance measurements are performed to determine the SCR width. The high frequency avoids the capacitance contribution from surface defects and deep levels within the bulk [26]. From the Mott-Schottky plot [38] of the CIGS cell [Fig. 4(b)], the SCR width W at no applied bias ($V = 0$ V) is determined to be 420 nm using the relative dielectric constant $\epsilon_r = 12$ for the CIGS layer [19,39]. Additionally, the built-in potential is determined to be 0.60 V and the hole concentration is 4.6×10^{15} cm^{-3}. The reflectance R_{ab} from the CIGS front surface is measured using a UV-visible spectrometer [Fig. 4(c)]. The fabricated CIGS solar cell with a structure of

TABLE I. The values of $\alpha, i_{\mathrm{LP}}, I_L, R_{\mathrm{ab}}$, and $i_{\mathrm{LP}}hc/2\pi r_o eI_L(1-R_{\mathrm{ab}})\alpha\lambda$ at various λ are summarized for $t = 2\,\mu$m, $r_o = 1$ mm, and $W = 420$ nm for the fabricated CIGS test pattern.

λ(nm)	α(m^{-1})	i_{LP}(A)	I_L(Wm^{-2})	R_{ab}	$E \equiv \frac{i_{\mathrm{LP}}hc}{2\pi r_o eI_L(1-R_{\mathrm{ab}})\alpha\lambda}$ (m^2)
700	7.36×10^6	8.07×10^{-7}	1.26×10^2	0.19	3.02×10^{-13}
800	5.65×10^6	7.25×10^{-7}	9.92×10^1	0.19	3.93×10^{-13}
900	3.77×10^6	1.28×10^{-6}	1.63×10^2	0.19	5.64×10^{-13}
970	2.97×10^6	4.38×10^{-8}	6.69×10^0	0.20	5.60×10^{-13}
1000	2.51×10^6	8.85×10^{-8}	1.51×10^1	0.18	5.62×10^{-13}
1025	2.02×10^6	2.04×10^{-7}	4.48×10^1	0.18	5.29×10^{-13}
1050	1.46×10^6	1.27×10^{-7}	6.88×10^0	0.25	3.16×10^{-13}

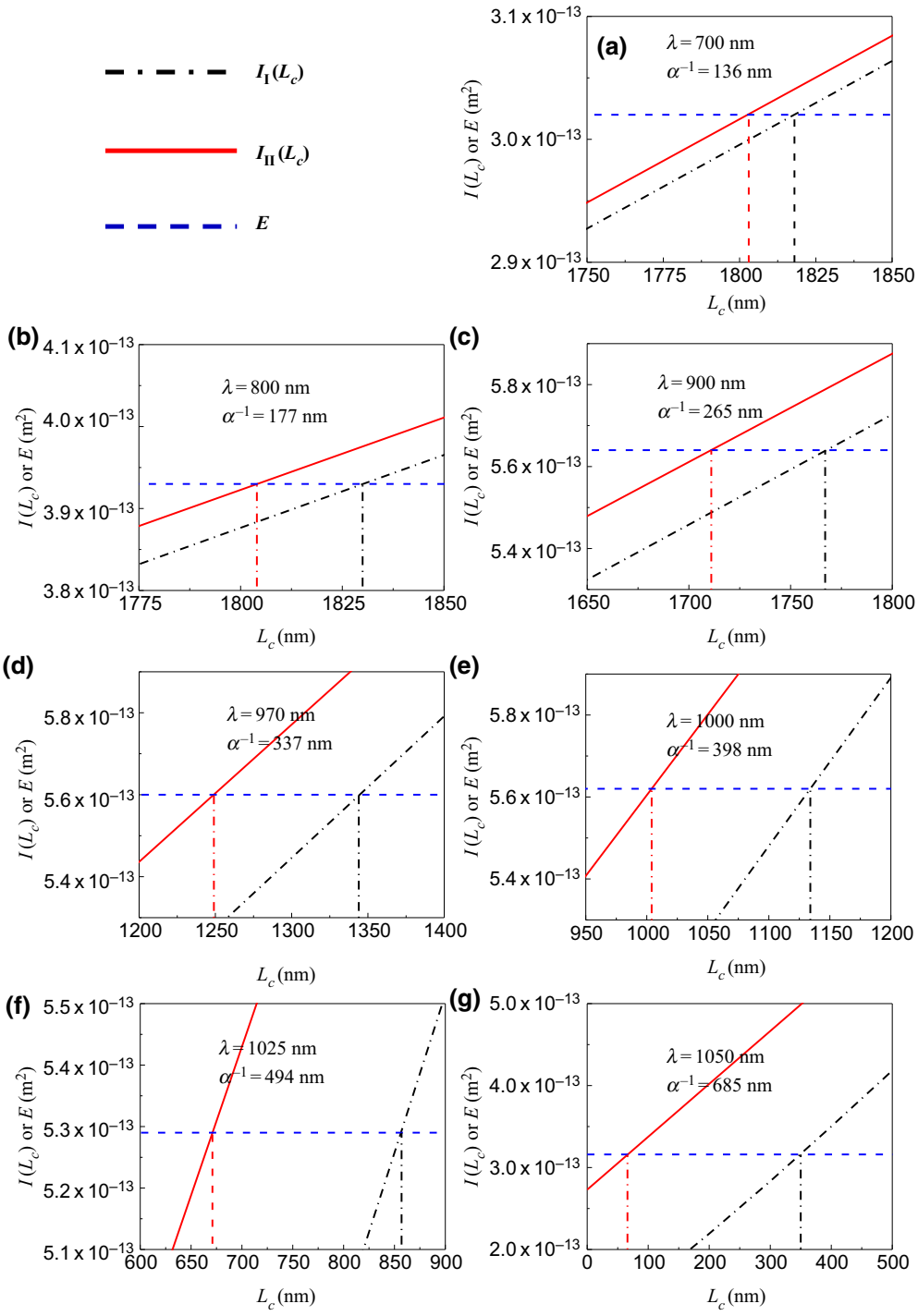

FIG. 5. Determination of the L_c values at various λ for two extreme cases: case I and II. (a)–(g) The calculated $\mathbf{I_I}$ and $\mathbf{I_{II}}$ as a function of L_c, and the experimentally obtained **E** values at various λ. The corresponding λ and α^{-1} values are written as an inset in each curve.

ZnO:Al/*i*-ZnO/CdS/CIGS/Mo shows a power conversion efficiency of 17.2%, an open-circuit voltage of 0.673 V, a short-circuit current density of 34.2 mA/cm^2, and a fill factor of 74.9%.

The i_{LP} values are measured using a short-circuited source meter in the CIGS test pattern under narrow-bandwidth light [Fig. 4(a)]. A narrow-bandwidth (10 or 50 nm) light is generated by passing white light through optical band-pass filters. The I_L values are measured by an optical power meter. The values of $\alpha, i_{LP}, I_L, R_{ab}$, and $i_{LP}hc/2\pi r_o e I_L(1-R_{ab})\alpha\lambda$ at various λ are summarized (Table I). Values for $\alpha(\lambda)$ are obtained for the CIGS layer

(with a band gap of 1.17 eV) from Paulson *et al*. [40]. The values of i_{LP}, I_L, R_{ab}, and W are measured in this work.

B. Step-by-step procedure for determining L_c depth profiles for a graded-band-gap CIGS solar cell

The step-by-step procedure with the theoretical relation and the experimental data for determining the L_c depth profile of the CIGS cell is described here. The procedure for determining the L_c depth profile is explained in four steps. The entire left-hand side $i_{LP}hc/2\pi r_o eI_L(1-R_{ab})\alpha\lambda$ in Eqs. (7) and (11) is denoted **E** for the experimentally obtained value, and the entire right-hand side in Eqs. (7) and (11), composed of double integrals, is denoted $\mathbf{I_I}$ for the integral of case I and $\mathbf{I_{II}}$ for case II. The first step is to generate curves of $\mathbf{I_I}$ and $\mathbf{I_{II}}$ as a function of L_c at a certain wavelength (for example, $\lambda = 700$ nm). The second step is to draw a horizontal line with the experimentally obtained **E** at $\lambda = 700$ nm, 3.02×10^{-13} m^2, on the graph [Fig. 5(a)]. The **E** values at various λ are shown in Table I. The third step is to determine the L_c values satisfying the conditions $\mathbf{E} = \mathbf{I_I}$ and $\mathbf{E} = \mathbf{I_{II}}$. Vertical lines are drawn from the points at $\mathbf{E} = \mathbf{I_I}$ and $\mathbf{E} = \mathbf{I_{II}}$ to the L_c axis. Thus, $L_c(\alpha^{-1} = 136\,\text{nm at}\,\lambda = 700\,\text{nm})$ is determined to be 1818 nm for case I and 1803 nm for case II. The final step is to repeat steps 1–3 for different λ values (seven wavelengths in this work). The corresponding λ and α^{-1} values are indicated as an inset in each curve [Figs. 5(a)–5(g)]. All extracted L_c values are gathered to provide the L_c depth profiles for the two cases (Fig. 6).

C. Recombination characteristics of minority carriers for graded-band-gap CIGS

The real depth-resolved L_c profile of the fabricated graded-band-gap CIGS solar cell will be positioned in the marked area between the two determined L_c depth profiles obtained from cases I and II (Fig. 6). Over the absorption depth of 177 nm, L_c is observed to remain nearly constant between 1803 and 1830 nm. L_c rapidly decreases beyond a depth of 265 nm, and reaches the values of 66–350 nm at a depth of 685 nm. The minority carriers generated in the deeper CIGS region have a higher probability of diffusing to the back surface and get recombined, and the L_c values at the deeper regions become significantly lower. The monotonically increase of L_c with increasing distance from the back surface d (top axis of Fig. 6) is due to the effect of the back surface recombination getting weaker. When the minority carriers are generated further than L_d from the back surface, a significantly large fraction of the generated minority carriers cannot reach the back surface, and thus their recombination is negligibly affected by the back surface. When the distance d is larger than approximately 1800 nm, the L_c value is saturated to the value of 1803–1830 nm and remains unchanged with depth, reflecting that the effect of the back-surface recombination is negligible in that range. In addition, the minority carriers travel almost only in the r direction to reach the collecting electrode in that range ($d \geq 1800\,\text{nm}, \alpha^{-1} \leq 200\,\text{nm}$), which almost corresponds to one-dimensional diffusion. Therefore, L_c in that range corresponds to L_d because $L_d \cong L_{\text{eff}} \cong L_c$ when the back surface negligibly affects the recombination and the carriers also diffuse in one dimension [15,19,21,32]. As a result, the L_d value can be determined to be 1803–1830 nm, which is a reasonable result for CIGS solar cells [19,29,30].

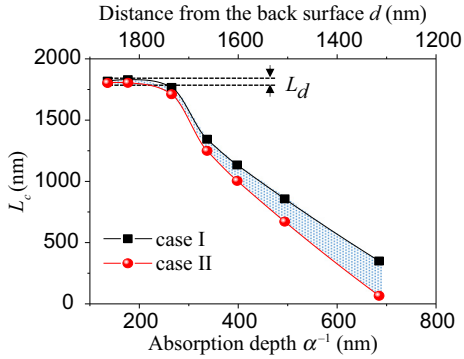

FIG. 6. The L_c depth profiles for the two extreme cases. The real L_c depth profile of the fabricated graded-band-gap CIGS solar cell will be positioned in the marked area between the determined two L_c depth profiles.

The next step is to determine the S_b value, which can be deduced from the measured depth-dependent L_c and the determined L_d of 1803–1830 nm. When minority charge carriers travel in the direction that is parallel to the four side surfaces in a square cylindrical semiconductor where each surface has same the surface recombination velocity $S_i (S_1 = S_2 = S_3 = S_4)$ [Fig. 7(a)], the relation between L_d, S_b, and L_{eff} derived by Brendel and Rau [41,42], is given by Eq. (12)

$$L_{\text{eff}} = \left(L_d^{-2} + \frac{1}{4}\frac{4S_i}{(G/2)D} \right)^{-(1/2)}, \tag{12}$$

where S_i is the surface recombination velocity at each surface, $G/2$ is the distance from the center (average position of the carriers) of the square cross section to each interface, and D is the diffusivity of the minority carrier.

In the case of $S_1 = S_2 = S_3 = 0$, $S_4 = S_b$, and $G/2 = d$, $4S_i$ and $G/2$ are replaced by S_b and d, respectively, in Eq. (12), and we thus obtain Eq. (13), which describes the relation between L_d, S_b, and L_{eff} when minority charge carriers travel in the direction, which is parallel to the bottom side surface [Fig. 7(b)].

$$L_{\text{eff}} = \left(L_d^{-2} + \frac{1}{4}\frac{S_b}{dD} \right)^{-(1/2)} \tag{13}$$

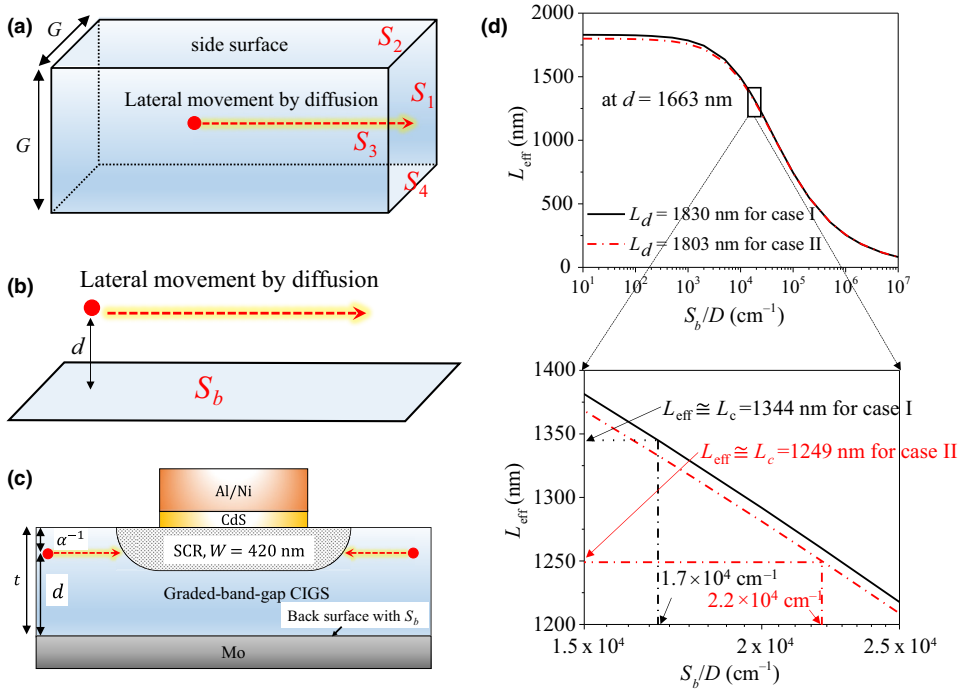

FIG. 7. Determination of the CIGS/Mo back-surface recombination velocity S_b. (a) A schematic of charge carriers traveling by diffusion parallel to the four-sided surfaces in a square cylindrical semiconductor for reference to Eq. (12). (b) A schematic of charge carriers traveling by diffusion parallel to the bottom surface for reference to Eq. (13). (c) A schematic of the charge carriers traveling by diffusion in the horizontal direction in the CIGS test pattern. (d) Determination of S_b/D for the graded-band-gap CIGS solar cell from the plots of L_{eff} vs S_b/D and the two measured L_c values at $d = 1663$ nm for two extreme cases.

Equation (13) can be applied for the custom-designed structure by substituting $t - \alpha^{-1}$ for d where t is the thickness of the CIGS layer and α^{-1} is the absorption depth corresponding to the average position for the photogeneration of the minority carriers [Fig. 7(c)]. Here, the effect of the front-surface recombination is neglected because the bare CIGS front-surface recombination velocity has been reported to be negligibly small compared to the CIGS/Mo back-surface recombination velocity, and the reported value of approximately 10^3 cm/s for the front-surface recombination velocity is expected to have virtually no effect on device performance [43–45].

To appropriately extract S_b by employing Eq. (13), the movement of carriers should be nearly horizontal. Therefore, the absorption depth should be smaller than the SCR width ($W = 420$ nm in this work). Otherwise, the displacement of the minority carrier inevitably includes the vertical component, which, in turn, should cause the extraction of incorrect values of S_b. In other words, the diffusional motion should be almost one-dimensional, in which $L_{\text{eff}} \cong L_c$, as mentioned in Sec. I. As a result, we can replace L_{eff} by L_c in Eq. (13) for absorption smaller than W. In addition, the drop in the L_c value due to S_b must be clearly observed. We have these two choices, which satisfy the above conditions. One is L_c at $d = 1663$ nm, and the other is L_c at $d = 1602$ nm [Figs. 6 and 7(c)].

Figure 7(d) shows calculated $L_{\text{eff}}(\cong L_c)$ values as a function of S_b/D at $d = 1663$ nm using Eq. (13) for the two L_d values: the upper limit (1830 nm for case I) and the lower limit (1803 nm for case II). From the determined values of $L_c = 1344$ nm (case I) and $L_c = 1249$ nm (case II) at $d = 1663$ nm, S_b/D is determined to be 1.7×10^4–2.2×10^4 cm^{-1} [Fig. 7(d)]. In the same way, S_b/D is to be 3.1×10^4–4.3×10^4 cm^{-1} at $d = 1602$ nm. Thus, the S_b/D value is expected to be 1.7×10^4–4.3×10^4 cm^{-1}. The extracted values agree well with the previously reported value for graded CIGS solar cells [26]. The minority carrier mobility has been estimated to be approximately 100 cm^2/Vs in CIGS solar cells [3]. The D value is thus estimated to be 2.57 cm^2/s at room temperature using the Einstein equation $D = (\mu kT/e)$, where k is the Boltzmann constant, T is the absolute temperature, e is the electron charge, and μ is the drift mobility. Thus, S_b is estimated to be 4.4×10^4–1.1×10^5 cm/s for the fabricated graded-band-gap CIGS solar cell.

V. SUMMARY

In summary, a wavelength-dependent lateral photocurrent method is developed to characterize both L_d and S_b for graded-band-gap solar cells. Graded-band-gap solar cells exhibit a mixture of charge carrier drift and diffusion,

which makes it difficult to determine the recombination properties of the minority carrier using standard methods. The functions $i_{LP} = i_{LP}(L_c)$ are theoretically derived using a generic custom-designed device structure. From the measured wavelength-dependent i_{LP} values and the derived functions $i_{LP} = i_{LP}(L_c)$, the depth-dependent L_c values are obtained for a graded-band-gap CIGS solar cell as a test demonstration of this method. Based on the L_c depth profiles, the L_d and S_b of the graded-band-gap CIGS cell are determined with reasonable values of 1803–1830 nm and 4.4×10^4–1.1×10^5 cm/s, respectively. This work is expected to be readily applicable to emerging graded-band-gap solar cells, including perovskite and $Cu_2ZnSn(S, Se)_4$ solar cells and to other photoactive devices, such as photodetectors and photoelectrochemical water-splitting devices, because this approach does not require the depth profile of the band gap of the light absorber in solar cells.

ACKNOWLEDGMENTS

This research was supported by Basic Science Research Program through the National Research Foundation of Korea (NRF) funded by the Ministry of Science and ICT (Grant No. NRF-2019R1F1A1058917), and by the Ministry of Education (Grant No. NRF-2016R1D1A1B03934840). The author thanks Professor Ki-Ha Hong (Hanbat National University) for helpful discussions.

[1] J. Mattheis, P. J. Rostan, U. Rau, and J. H. Werner, Carrier collection in Cu(In, Ga)Se_2 solar cells with graded band gaps and transparent ZnO:Al back contacts, Sol. Energy Mater. Sol. Cells **91**, 689 (2007).

[2] M. Contreras, J. Tuttle, D. Du, Y. Qi, A. Swartzlander, A. Tennant, and R. Noufi, Graded band-gap Cu(In, Ga)Se_2 thin-film solar cell absorber with enhanced open-circuit voltage, Appl. Phys. Lett. **63**, 1824 (1993).

[3] D. Kuciauskas, J. V. Li, M. A. Contreras, J. Pankow, P. Dippo, M. Young, L. M. Mansfield, R. Noufi, and D. Levi, Charge carrier dynamics and recombination in graded band gap $CuIn_{1-x}Ga_xSe_2$ polycrystalline thin-film photovoltaic solar cell absorbers, J. Appl. Phys. **114**, 154505 (2013).

[4] K. J. Yang, D. H. Son, S. J. Sung, J. H. Sim, Y. I. Kim, S. N. Park, D. H. Jeon, J. Kim, D. K. Hwang, C. W. Jeon, D. Nam, H. Cheong, J. K. Kang, and D. H. Kim, A band-gap-graded CZTSSe solar cell with 12.3% efficiency, J. Mater. Chem. A **4**, 10151 (2016).

[5] K. Woo, Y. Kim, W. Yang, K. Kim, I. Kim, Y. Oh, J. Y. Kim, and J. Moon, Band-gap-graded $Cu_2ZnSn(S_{1-x}, Se)_x)4$ solar cells fabricated by an ethanol-based particulate precursor ink route, Sci. Rep. **3**, 3069 (2013).

[6] S. J. Yun, J. K. Kim, and J. W. Lim, Amorphous SiGe:H thin film solar cells with light absorbing layers of graded bandgap profile, Electrochem. Solid-State Lett. **15**, B9 (2011).

[7] H. Bian, D. Bai, Z. Jin, K. Wang, L. Liang, H. Wang, J. Zhang, Q. Wang, and S. (Frank) Liu, Graded bandgap $CsPbI_{2+x}Br_{1-x}$ perovskite solar cells with a stabilized efficiency of 14.4%, Joule **2**, 1500 (2018).

[8] C. Chen, Z. Song, C. Xiao, D. Zhao, N. Shrestha, C. Li, G. Yang, F. Yao, X. Zheng, R. J. Ellingson, C.-S. Jiang, M. Al-Jassim, K. Zhu, G. Fang, and Y. Yan, Achieving a high open-circuit voltage in inverted wide-bandgap perovskite solar cells with a graded perovskite homojunction, Nano Energy **61**, 141 (2019).

[9] O. Ergen, S. M. Gilbert, S. J. Turner, and A. Zettl, Hexagonal boron nitride as a cationic diffusion barrier to form a graded bandgap perovskite heterostructure, Phys. Status Solidi B **253**, 2478 (2016).

[10] F. Fu, S. Pisoni, T. P. Weiss, T. Feurer, A. Wäckerlin, P. Fuchs, S. Nishiwaki, L. Zortea, A. N. Tiwari, and S. Buecheler, Compositionally graded absorber for efficient and stable near-infrared-transparent perovskite solar cells, Adv. Sci. **5**, 1700675 (2018).

[11] U. Rau, B. Blank, T. C. M. Müller, and T. Kirchartz, Efficiency Potential of Photovoltaic Materials and Devices Unveiled by Detailed-Balance Analysis, Phys. Rev. Appl. **7**, 044016 (2017).

[12] J. P. Teixeira, R. A. Sousa, M. G. Sousa, A. F. Da Cunha, P. A. Fernandes, P. M. P. Salomé, and J. P. Leitão, Radiative transitions in highly doped and compensated chalcopyrites and kesterites: The case of Cu_2ZnSnS_4, Phys. Rev. B **90**, 235202 (2014).

[13] M. Lang, C. Zimmermann, C. Krämmer, T. Renz, C. Huber, H. Kalt, and M. Hetterich, Luminescence properties of $Cu_2ZnSn(S, Se)_4$ solar cell absorbers: State filling versus screening of electrostatic potential fluctuations, Phys. Rev. B **95**, 155202 (2017).

[14] J. H. Werner, S. Kolodinski, U. Rau, J. K. Arch, and E. Bauser, Silicon solar cell of 16.8 μm thickness and 14.7% efficiency, Appl. Phys. Lett. **62**, 2998 (1993).

[15] C. J. Hages, N. J. Carter, and R. Agrawal, Generalized quantum efficiency analysis for non-ideal solar cells: Case of $Cu_2ZnSnSe_4$, J. Appl. Phys. **119**, 014505 (2016).

[16] C. Hu and D. Clifford, Determination of diffusion Length and surface recombination velocity by light excitation, Solid State Electron. **21**, 965 (1978).

[17] J. Parisi, D. Hilburger, M. Schmitt, and U. Rau, Quantum efficiency and admittance spectroscopy on Cu(In, Ga)Se_2 solar cells, Sol. Energy Mater. Sol. Cells **50**, 79 (1998).

[18] D. Ritter, E. Zeldov, and K. Weiser, Steady-state photocarrier grating technique for diffusion length measurement in photoconductive insulators, Appl. Phys. Lett. **49**, 791 (1986).

[19] T. Gokmen, O. Gunawan, and D. B. Mitzi, Minority carrier diffusion length extraction in $Cu_2ZnSn(Se, S)_4$ solar cells, J. Appl. Phys. **114**, 114511 (2013).

[20] R. Shikler, N. Fried, T. Meoded, and Y. Rosenwaks, Measuring minority-carrier diffusion length using a Kelvin probe force microscope, Phys. Rev. B **61**, 11041 (2000).

[21] X. X. Liu and J. R. Sites, Solar-cell collection efficiency and its variation with voltage, J. Appl. Phys. **75**, 577 (1994).

[22] R. Scheer, M. Wilhelm, and H. J. Lewerenz, Measurements of minority-carrier diffusion length in n-$CuInS_2$ by electron-beam-induced current method, J. Appl. Phys. **66**, 5412 (1989).

[23] D. E. Ioannou and C. A. Dimitriadis, A SEM-EBIC minority-carrier diffusion-length measurement technique, IEEE Trans. Electron Devices **29**, 445 (1982).

[24] K. L. Luke and L. J. Cheng, Analysis of the interaction of a laser pulse with a silicon wafer: Determination of bulk lifetime and surface recombination velocity, J. Appl. Phys. **61**, 2282 (1987).

[25] G. S. Kousik, Z. G. Ling, and P. K. Ajmera, Nondestructive technique to measure bulk lifetime and surface recombination velocities at the two surfaces by infrared absorption due to pulsed optical excitation, J. Appl. Phys. **72**, 141 (1992).

[26] G. Brown, V. Faifer, A. Pudov, S. Anikeev, E. Bykov, M. Contreras, and J. Wu, Determination of the minority carrier diffusion length in compositionally graded Cu(In, Ga)Se_2 solar cells using electron beam induced current, Appl. Phys. Lett. **96**, 2 (2010).

[27] I. Repins, M. A. Contreras, B. Egaas, C. DeHart, J. Scharf, C. L. Perkins, B. To, and R. Noufi, 19.9%-efficient ZnO/CdS/$CuInGaSe_2$ solar cell with 81.2% fill factor, Prog. Photovoltaics Res. Appl. **16**, 235 (2008).

[28] S. Niki, M. Contreras, I. Repins, M. Powalla, K. Kushiya, S. Ishizuka, and K. Matsubara, CIGS absorbers and processes, Prog. Photovoltaics Res. Appl. **18**, 453 (2010).

[29] R. Scheer, M. Wilhelm, H. J. Lewerenz, H. W. Schock, and L. Stolt, Determination of charge carrier collecting regions in chalcopyrite heterojunction solar cells by electron-beam-induced current measurements, Sol. Energy Mater. Sol. Cells **49**, 299 (1997).

[30] R. Scheer, C. Knieper, and L. Stolt, Depth dependent collection functions in thin film chalcopyrite solar cells, Appl. Phys. Lett. **67**, 3007 (1995).

[31] D. K. Schroder, *Semiconductor Material and Device Characterization* (John Wiley & Sons, New York, 1990).

[32] A. Kumar, Predicting efficiency of solar cells based on transparent conducting Electrodes, J. Appl. Phys. **121**, 014502 (2017).

[33] S. G. Balster, D. K. Schroder, J. Bailey, and J. P. Kalejs, In situ gettering of edge-defined film-fed growth silicon in a CO ambient, J. Appl. Phys. **77**, 371 (1995).

[34] V. Thuong-Quat, W. Eichhammer, and P. Siffert, Inhomogeneous defect activation by rapid thermal processes in ilicon, Appl. Phys. Lett. **54**, 1235 (1989).

[35] R. F. Pierret, *Field Effect Devices* (Addison-Wesley, Reading, MA, 1990).

[36] S. Lee, K. S. Cho, S. Song, K. Kim, Y. J. Eo, J. H. Yun, J. Gwak, and C. H. Chung, Fabrication of robust nanoscale contact between a silver nanowire electrode and CdS buffer layer in Cu(In, Ga)Se_2 thin-film solar cells, J. Vis. Exp. **149**, e59909 (2019).

[37] S. Lee, J. S. Lee, J. Jang, K. H. Hong, D. K. Lee, S. Song, K. Kim, Y. J. Eo, J. H. Yun, J. Gwak, and C. H. Chung, Robust nanoscale contact of silver nanowire electrodes to semiconductors to achieve high performance chalcogenide thin film solar cells, Nano Energy **53**, 675 (2018).

[38] C. Adel, B. M. Fethi, and B. Brahim, Optical and electrical characterization of CIGS thin films grown by electrodeposition route, Optik (Stuttg) **127**, 4118 (2016).

[39] J. Lee, J. D. Cohen, and W. N. Shafarman, The determination of carrier mobilities in CIGS photovoltaic devices using high-frequency admittance measurements, Thin Solid Films **480–481**, 336 (2005).

[40] P. D. Paulson, R. W. Birkmire, and W. N. Shafarman, Optical characterization of $CuIn_{1-x}Ga_xSe_2$ alloy thin films by spectroscopic ellipsometry, J. Appl. Phys. **94**, 879 (2003).

[41] R. Brendel and U. Rau, Injection and collection diffusion lengths of polycrystalline thin-film solar cells, Solid State Phenom. **67–68**, 81 (1999).

[42] R. Scheer and H.-W. Schock, *Chalcogenide Photovoltaics: Physics, Technologies, and Thin Film Devices* (Wiley-VCH, New York, 2011).

[43] W. K. Metzger, I. L. Repins, and M. A. Contreras, Long lifetimes in high-efficiency Cu(In, Ga)Se_2 solar cells, Appl. Phys. Lett. **93**, 23 (2008).

[44] W. K. Metzger, I. L. Repins, M. Romero, P. Dippo, M. Contreras, R. Noufi, and D. Levi, Recombination kinetics and stability in polycrystalline Cu(In, Ga)Se_2 solar cells, Thin Solid Films **517**, 2360 (2009).

[45] I. Repins, S. Glynn, J. Duenow, T. J. Coutts, W. K. Metzger, and M. A. Contreras, Required materials properties for high-efficiency CIGS modules, Proc. SPIE **7409**, 74090M (2009).